The effect of a promontory on the passive tracers advected by a coastal current: A full three-dimensional numerical study(*)

G. Leuzzi(^{1})(**) and R. Purini(^{2})

(^{1}) *Dipartimento di Idraulica, Trasporti e Strade, Università di Roma "La Sapienza"*
   via Eudossiana, 18, 00184 Rome, Italy
(^{2}) *CNR, ISAC - via del Fosso del Cavaliere, 100, 00133 Rome, Italy*

Summary. — The coupling of a community three-dimensional primitive equation model with a three-dimensional Lagrangian dispersion model is used to describe with sufficient accuracy the temporal and spatial evolution of passive tracers released along a coast characterized by the presence of a cape. The simulations show how different initial conditions influence dispersion properties in a stratified sea, also to provide some insight on the valuation of the environmental impact of pollutants released along the coast. Finally, the power spectra content in a well-defined frequency range of the internal gravity waves is interpreted on the basis of vortex shedding in the lee of the promontory.

PACS `92.10.Lq` – Turbulence and diffusion.
PACS `92.10.Sx` – Coastal and estuarine oceanography.
PACS `92.20.Ny` – Marine pollution.

1. – Introduction

In recent times, coastal areas have been at the centre of growing interest because the increased economic and political role of these parts of the world ocean. This fact originated studies in many disciplines ranging from the economy to different branches of the exact sciences and, in particular, to the physical oceanography. Regarding the latter research field, it is worth to underline that coastal processes show remarkable differences with respect to the open ocean ones because the relevance of the sea floor on the ocean dynamics, the presence of the coast that induces, for example, strong variations of the sea level, the role of the vertical stratification as resulting from the high variability of air-sea fluxes and son on. For all these reasons, the coastal ocean has been defined "... among

___

(*) The authors of this paper have agreed to not receive the proofs for correction.
(**) E-mail: giovanni.leuzzi@uniroma1.it

the most challenge marine environment of the world" [1]. To cope with this challenge, in the two last decades more and more studies, and in particular numerical ones, have been addressed to both basic mechanisms and the understanding of flow properties for specific coasts [1]. However, (relatively) few of these studies have focused the interaction of coastal current with a cape and yet fewer when this kind of physical setting is associated with the transport of passive tracers. An exception to this remark is provided by a recent paper that presents some numerical simulations, for a homogeneous sea, of the dispersion of wastes released by a fish farm located near the Portofino promontory (Italy) [2]. With the aim to generalize this approach to a stratified flow at mid-latitude, the present study furnishes some preliminary results by combining a community three-dimensional ocean model with a three-dimensional dispersion model, that is the marine adaptation of a model originally developed for the atmospheric boundary layer [3, 4].

The second section, after a short description of the three-dimensional hydrodynamical model POM (Princeton Ocean Model), presents the physical settings for the study area. In the third section the dispersion model LASEMOD (LAgrangian SEa MODel) is briefly presented. The fourth section shows different dynamical fields obtained by varying both Burger and Reynolds numbers and the direction of the current impinging the promontory. The fifth section presents the three-dimensional simulations of the dispersion of pollutants considered as passive scalars. The sixth section provides some considerations about the origin of the wavy patterns that affect the present simulations giving in the mean time an explanation about the power spectra content for some grid points close to the coast. Finally, the last section presents, in connection with concluding remarks, some indications for further studies.

2. – The three-dimensional coastal model and its physical set-up

The POM is a three-dimensional, free surface, sigma coordinate, primitive equation ocean model which includes a turbulence sub-model [5]. It was developed in the late 1970's with subsequent contributions from other people. More technical details and the list of the POM publications can be found in the Princeton Ocean Model Web site.

The present application refers to the integration domain of rectangular shape having dimensions 48 km × 100 km (fig. 1). The y-axis, pointing northward, is aligned along the direction of the coast (which is on the right side of the domain) and the x-axis points to the coast; therefore, the z-axis is negative for increasing the depth. Clearly, the western boundary represents the open sea although, to optimize the dynamical boundary conditions (BCs), is considered as a solid boundary since the BCs there do not affect significantly the dynamics in the area of interest, *i.e.* that closer to the coast. This area, 50 km far from the southern boundary, is centred around the rectangle of dimensions 4 km × 5 km representing the side protruding into the sea and the base of the promontory, respectively. Both southern and northern boundaries are considered open since they represent the entrance and exit sections (and vice versa) respectively of the coastal flow. In these boundaries the BCs for the horizontal velocities are radiative as prescribed by Orlanski's scheme [6], unless for the averaged velocity in the southern boundary where Flather's boundary condition [7] is applied. To describe with accuracy the coastal dynamics, the grid is taken variable along the x direction starting from 200 m (close to the coast) to arrive at 1 km in correspondence of the western boundary. Differently, the grid mesh is considered constant and equal to 0.5 km for the y-axis. Finally, the bathymetry has been schematised by means of a monotonic function reaching a depth of 66 m at 20 km off shore (fig. 1).
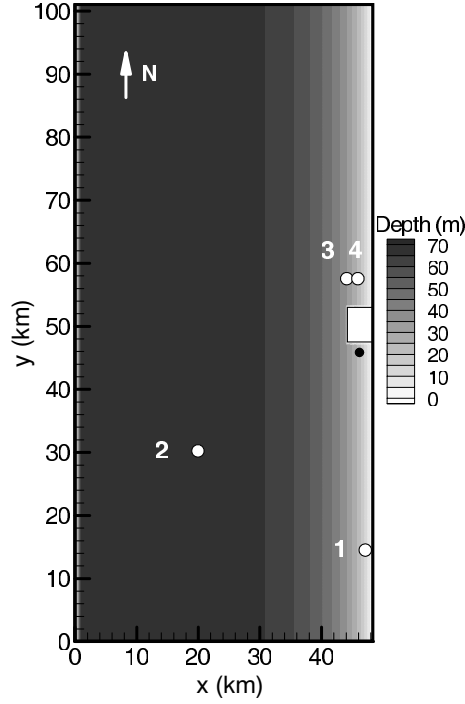
Fig. 1. – The bathymetry in the integration domain. The white rectangle and the black circle represent the promontory and the pollutant source, respectively. Nodes 1-4 (white circles) are chosen for the internal waves analysis.

The initial and incoming horizontal velocity is assumed initially vertically homogeneous. Differently, the initial temperature is assumed to vary along the vertical and with such an assumption it is possible to understand the dynamical effect of Brunt-Väisälä changes. Please note that in the present simulations the density is assumed to be depending on the temperature alone. With the previous physical parameters the Burger number

$$(2.1) \qquad\qquad Bu = N^2 H^2 / f_C^2 L^2$$

is defined, where H is the characteristic depth (66 m), f_C the Coriolis parameter ($\approx 5 \times 10^{-5}$ s^{-1}), L the characteristic horizontal dimension (50 km) and N the Brunt-Väisälä frequency:

$$(2.2) \qquad\qquad N = \left(g\alpha \, \frac{\mathrm{d}T}{\mathrm{d}z} \right)^{1/2} ,$$

where α ($\approx 1.7 \times 10^{-4}$ K^{-1}) is the coefficient of thermal expansion. Analogously to the Signell and Rockell Geyer paper [8], it is then possible to define the equivalent Reynolds number:

$$(2.3) \qquad\qquad Re = H/DC_D ,$$

where D is the semi-amplitude of the promontory (2 km) and C_D is the bottom drag coefficient. Considered that the present simulations are obtained by varying both the current direction and the Brunt-Väisälä frequency (for constant equivalent Reynolds number), it is then possible to make a comparison between present results and those appearing in the literature [8-13]. It is worth noticing that the above physical settings, jointly with the location of the pollutant source and its intensity indicated in the next section, resemble the area around the Argentario promontory (central Italy) where environmental concerns are due to a fish farm located in the Ansedonia bay.

3. – The dispersion model LASEMOD

In the last two decades Lagrangian particle models have been extensively used for the assessment of aquatic dispersion problems. The applications range from marine waste-water discharges to the spreading of oil spills. A recent field of research is the dispersion of wastes from marine cage farms [2, 14]. The Lagrangian particle approach can give the following advantages: low numerical diffusion, high spatial resolution without increment of computational costs, each particle can be tagged with its specific characteristics (mass, size, deposition velocity, decay time, etc.), the hydrodynamic input can be furnished directly from simulated or measured data. Unfortunately measurements of marine turbulence are still scarcely available, reducing the potential of Lagrangian approach in the marine studies.

To authors' knowledge in all marine applications the particle velocities have been described by zero-order auto-regressive models. In such stochastic processes (defined "simple" random walk model), the next value of displacement depends on the current values, but the next velocity does not depend on the current one. As a consequence, simple random walk models can only describe processes for time steps larger than the integral time scale of the turbulent velocities. Such a conditions could be mismatched in convective conditions or when critical levels of concentration occur near the pollutant source. Generally speaking we may adopt simple random walk model when the size of the pollutant cloud is large respect to the integral spatial scale of the turbulence. Another limitation of the simple random walk model is the unrealistic collection of particles in zones with low velocity variances. Hunter *et al.* [15] give some indications to limit such a problem. Following this suggestion, Mead [16] utilises an additional "drift" velocity, proportional to the diffusivity gradient, but this method tends to accumulate particles in zones with high-velocity variances for large time steps.

In the attempt to overcome both the described limitations we have utilised LASE-MOD, that is a first-order autoregressive model for the velocities (*e.g.*, the turbulent velocities are time correlated). In such a way we can take account of the integral time scale of the turbulence, correctly resolving dispersion also in the vicinity of the pollutant source and for events with large turbulent eddies. Moreover LASEMOD is based on the "Well-Mixed" condition, formulated by Thomson [17], which states that particles of tracer initially well-mixed will remain so. This condition avoids the collection of particles in zones with low turbulence. LASEMOD is the oceanic development of a statistical Lagrangian model realised at the University of Rome "La Sapienza" for the atmospheric boundary layer [3, 4]. This model has been validated by comparison with theoretical solutions and field observations.

For marine applications the integral time scales, the mean velocities and variances can be deduced from the POM outputs. Because of the lack of turbulence similarity laws existing in literature for marine environment, the Turbulent Kinetic Energy (TKE) has

TABLE I. – *Physical settings of the currents for the four different simulations.*

Case	Current
A	northward baroclinic
B	northward barotropic
C	southward baroclinic
D	southward barotropic

been subdivided in velocity variances for each Cartesian direction following the atmospheric relationships [18]. According to Taylor's theory of dispersion [19], the Lagrangian time scale T_L has been obtained utilising the turbulence diffusivity k_m and the vertical velocity variance σ_w^2, by the simple relation

$$(3.1) \qquad\qquad T_L = k_m/\sigma_w^2\,;$$

LASEMOD utilises the same grid coordinate of the POM, with particle rebounds on grid boundaries of bottom and free surface. In the present simulation a pollutant point source with a constant mass rate Q (= 0.1 kg s^{-1}) has been adopted. The source is located at a distance of 2 km from the south side of the promontory (fig. 1), 2 m below the sea surface.

4. – Hydrodynamics results

Since the hydrodynamics determines the transport and dispersion of the embedded pollutants, in the following a short description of the flow characteristics for the case studies is presented.

The simulations refer to four different physical settings, all characterized by the same velocity $U = 0.2$ ms^{-1} for the inflow, but with different current directions and stratifications, as summarised in table I.

The temperature is assumed of 18 °C at the surface and decreasing by 4 °C at the depth of 66 m, giving a $N^2 \approx 1.36 \times 10^{-4}$ and $Bu \approx 9.5 \times 10^{-2}$. Finally, assuming C_D = 0.0025, the equivalent Reynolds number becomes $Re \approx 13$.

It is necessary to note that the case A corresponds to a late spring condition as deduced from a climatic atlas for the Italian coastal area surrounding the considered location [20].

After few hours of simulated time, an anticyclonic eddy lee of the promontory is formed and its amplitude grows in time for reaching approximately the same dimensions of the obstacle. Besides, the presence of the bottom slope induces an inhomogeneous distribution of the potential vorticity, that the swirling motion of the eddy redistributes. The fluid particles along the periphery of such a eddy are thus stretched and squeezed and develop vorticity anomalies that, in turn, do modify the main trajectory of the vortex. Therefore the fluid particles close to the promontory, moving in a water body of increasing depth, acquire positive vorticity generating a cyclone which, after 12 hours, tends to separate the anticyclone from the promontory. As a final result, this process generates a dipole like those presented in the literature [8, 11]. After the initial growth of the cyclone, a northward migration and decrease of both eddies is observed, although the latter effect seems to affect mainly the anticyclonic one. After 3 days approximately,
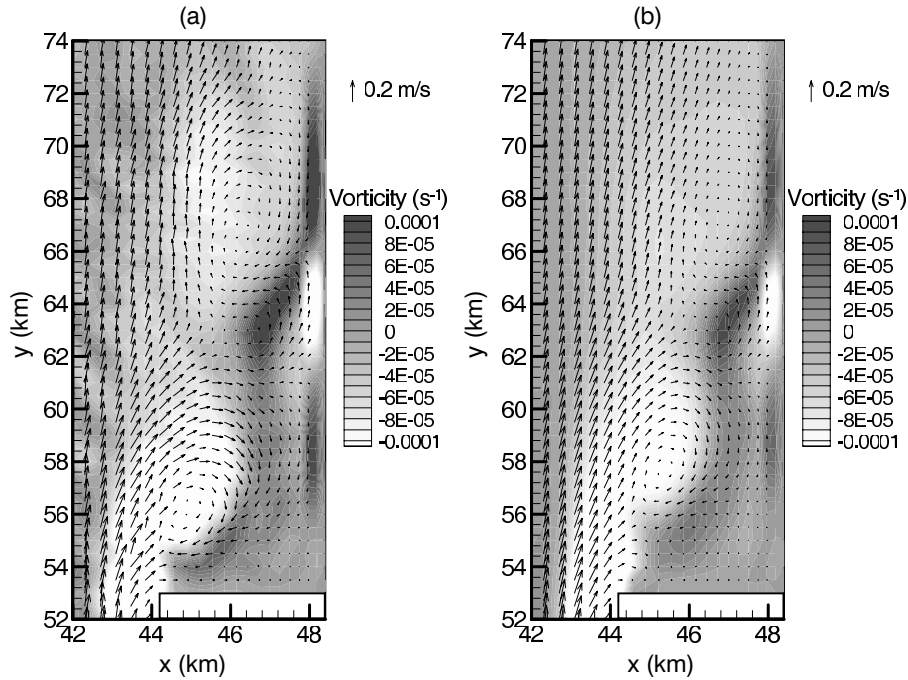
Fig. 2. – Surface velocity and vorticity fields in the lee of the promontory after 3 days of simulated time for the stratified (a) and isothermal northward current (b).

a new anticyclone is formed which is part of a vortex street characterized by a Strouhal number $St = f_r D_v / U \approx 0.2$, where f_r ($\approx 7.7 \times 10^{-6}$), D_v and U are the frequency of the vortices shed in the vortex street, the length scale and the above mean velocity, respectively. This result is in good agreement with that found in the classical theory of fluid dynamics [21]. The following evolution is dominated by the development of the bottom Ekman layer that induces quasi-steady conditions. For this phase, the presence of a wavy pattern due to internal gravity waves (thereinafter IGW) can be observed.

As for the previous situation, in the case B the formation of an intense anticyclonic vortex characterizes the early evolution process that is followed by the development of a cyclone which, separating the first eddy from the headland, produces a dipole by means of the same mechanisms described for the case A. However starting from the first day, the successive dynamics of the couple cyclone-anticyclone shows some differences with respect to those described above. In fact, the stratification of the previous case induces a greater instability of the primary anticyclone which initiates to undergo a fission while the cyclone remains sufficiently stable. This process of diversification increases with time until 3 days, while for longer time the similarities between cases A and B appear to be increased, although a lower vorticity does characterize the latter case with respect to the former (fig. 2). This similarity remains for the following days when the steady condition is achieved unless for the absence of IGW (fig. 2a) as the theory dictates for a homogeneous ocean [22].

The case C schematizes the same climatic condition of the first case, but for those particular meteorological events that are able to reverse the shelf current [2, 23]. For the
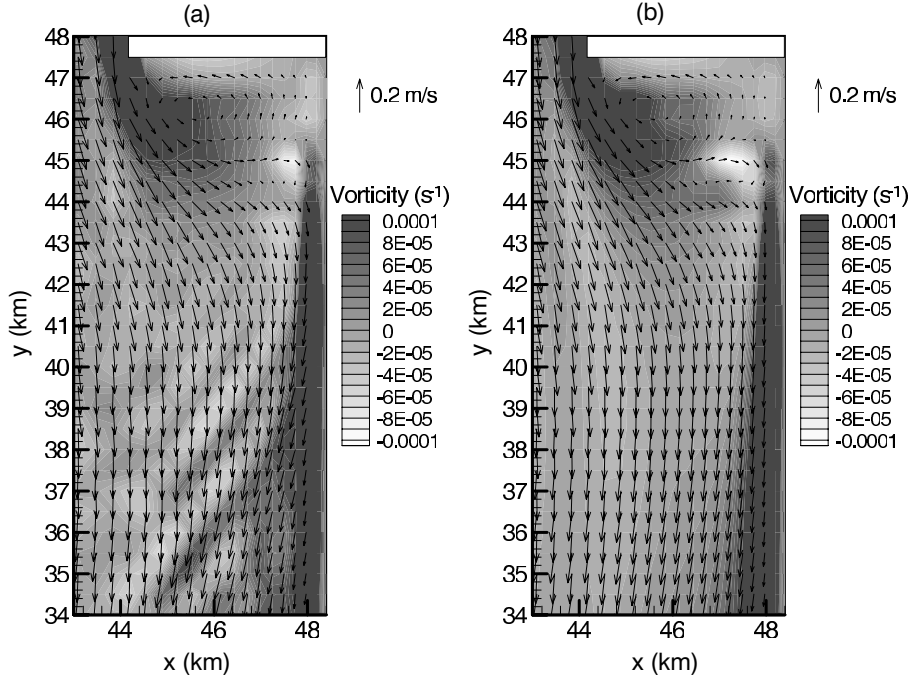
Fig. 3. – Surface velocity and vorticity fields in the lee of the promontory after 6 days of simulated time for the stratified (a) and isothermal southward current (b).

southward flow, the dynamics is quite different from that previous depicted. In fact, the cyclonic vortex develops quickly to a steady state and not apparently influenced by the presence of the small anticyclonic circulation between the cyclone and the promontory (fig. 3a). This event is in good agreement with laboratory experiments [10] for similar values of Bu and Re. The persistence of this cyclone can be explained as due to the secondary drift, *i.e.* its tendency to migrate, in the northern hemisphere, toward decreasing depth [24] and then, due to the presence of the promontory, to be locked in its initial position. Two final remarks: 1) the anticyclonic-vorticity–produced lee of the main vortex seems not influencing the whole dynamics and 2) the stratification induces again IGW (fig. 3a).

In the case D the dynamics of the cyclone is similar to that described in the case C unless for the absence of the IGW since the fluid is homogeneous (fig. 3b).

Giving some details on the thermodynamics, case A shows that the presence of the stratification induces a complex phenomenology which comprehends frontogenesis and the initial formation of cold filaments downstream the promontory, upwellings and the internal wave patterns. In the real world, these filaments assure the nutrification of the offshore surface waters by the upwelling of nutrient-rich bottom waters and/or the spreading on the surface waters of the pollutants released near the sea bottom.

Figure 4 shows the surface temperature distribution after 6 days of simulation. Upstream the promontory the temperature closer to the coast remains unchanged with respect to the inflow surface temperature, while lee of the promontory (10 km from the northern side) patches of cold surface waters are created following the phenomenology
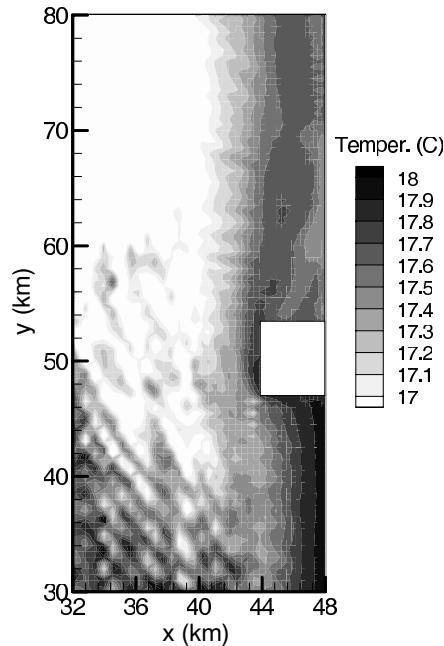
Fig. 4. – Surface temperature distribution for northward stratified current after 6 days of simulation.

briefly depicted above. Moreover, intense surface signatures of the IGW can be observed offshore.

For the turbulent diffusion coefficients, the POM computes the TKE using the closure turbulence model introduced by Mellor and Yamada [25]. Since this computation is depending on the vertical stratification of the sea, different behaviours characterize the stratified and homogeneous cases. In fact fig. 5a shows the TKE for the former one, indicating that the such a quantity, produced by viscosity in correspondence of the bottom layer, protrudes towards the surface with decreasing amplitude. A different behaviour marks the homogeneous case where layers of decreasing TKE are mainly aligned along the bottom until the TKE peak which corresponds to the horizontal maximum extension of the promontory (fig. 5b).

5. – Dispersion results

The hydrodynamical results obtained from the four cases simulated by POM have been utilised as input data from the coupled model LASEMOD. In each case 6 days of particle dispersion have been considered. The emission of pollutant started at the beginning of hydrodynamical simulation. Please note that the pollutant concentrations shown in the following refer to their vertically averaged value.

Initially, for the northward current, a plume parallel to the south side of the promontory forms. After 5 hours the plume bends around the cape and successively separates, following the mean current. The pollutant penetrates in the recirculation zone just behind the promontory. In the successive days the plume strongly spreads and inclines toward the coast following the mean current and the eddy shedding. In the case of
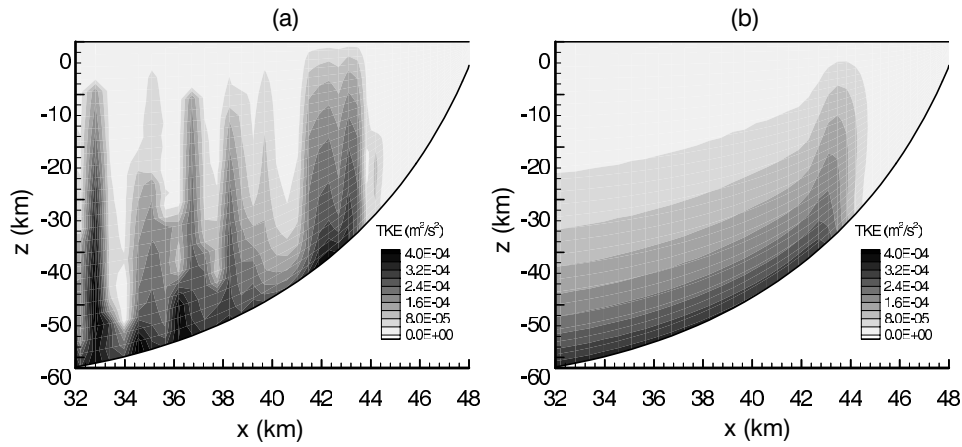
Fig. 5. – TKE at the cross-section $y = 57.5$ km for the stratified (a) and isothermal (b) northward current after 6 days of simulation.

stratified current (fig. 6a) high levels of concentration persist at long distances from the source and many particles enter in the recirculation zone behind the promontory. Such entrainment process is favoured by the more vigorous vortex shedding of the baroclinic current. A large number of particles remains trapped within vortices, giving rise to high
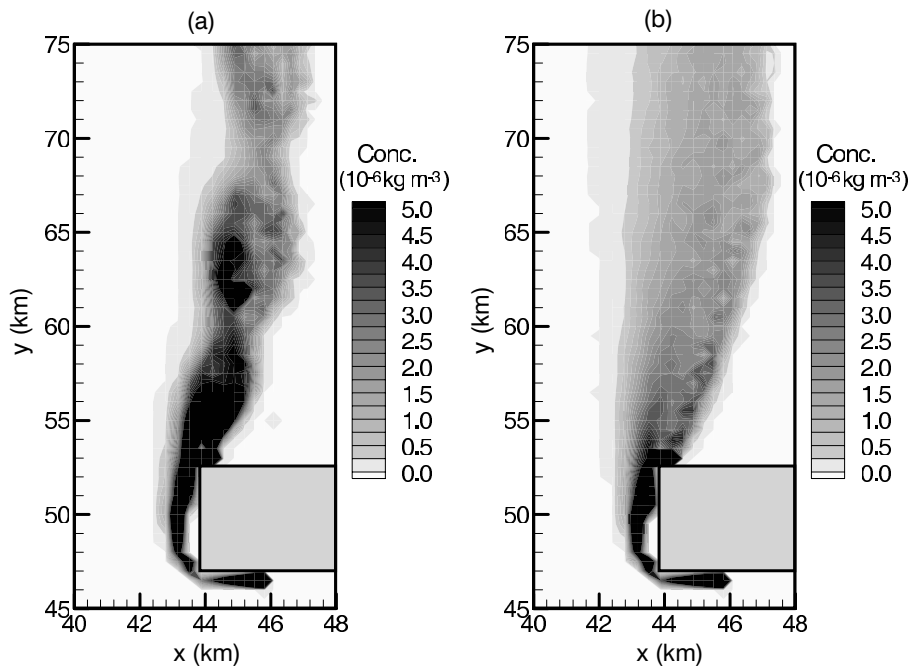

Fig. 6. – Depth-averaged concentrations of pollutant for stratified (a) and isothermal (b) northward current after 6 days of simulation.
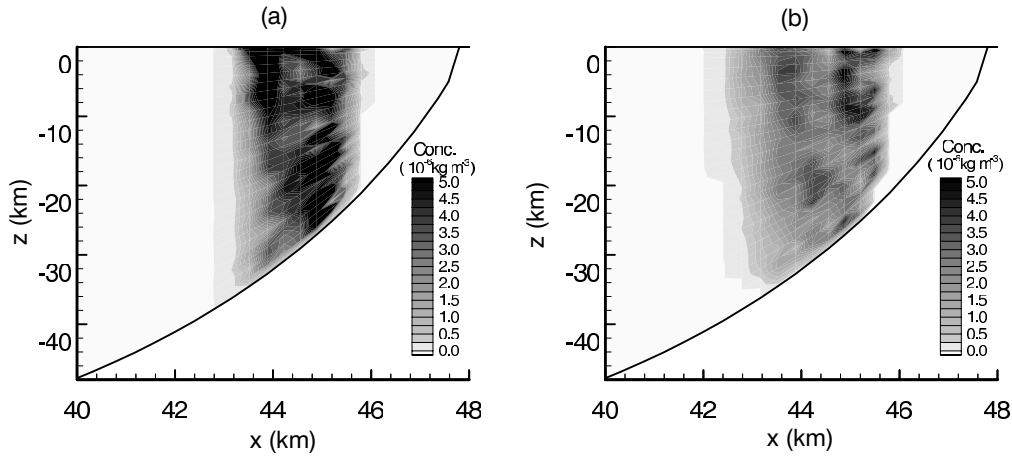
Fig. 7. – Concentrations of pollutant for stratified (a) and isothermal (b) northward current, calculated in a vertical section downstream to the promontory ($y = 57.5$ km) after 6 days of simulation.

levels of concentration far from the promontory. Such a behaviour is confirmed by the vertical section of the concentration field in the lee of the promontory (figs. 7a, b). All the particles are confined in a vertical column ranging from the bottom to the surface. In the case of baroclinic current the column is narrower and the concentration is higher (fig. 7a). The plume follows closely the main stream leaving some areas unaffected by the pollutants. Example of these areas can be seen on the head of the promontory, *i.e.* downstream the southern corner of the promontory. A second area is located lee of the promontory and close to the coast.

In the case of southward current a very different behaviour is evidenced. During the early hours the pollutant is transported parallel to the south side of the promontory, like in the previous case, but after the first corner, the plume is bent southward and gradually rotates toward the coast. In the successive hours a bifurcation occurs: one plume branch goes southward parallel to the coast and the other one goes in the opposite direction, forming an annular polluted area (fig. 8a). Such a behavior could not be well described by uncorrelated trajectory models, since tend to overestimate the pollutant spread near the source. The presence of stratification influences noticeably the southward propagation of the plume, which results separated from the coast differently from the barotropic case (fig. 8b). In the baroclinic case the plume is further split. One branch remains attached to the coast and the other one detaches. The vertical section of the concentration field (fig. 9a) shows that the offshore branch is confined near the bottom, pushed by a down welling current. The origin of this current might be attributed to the horizontal convergence of the currents at the sea surface (fig. 3a). In the barotropic case the Coriolis effect on the surface current is not evident and then there is not convergence (fig. 3b). A unique plume confined near the coast appears, as shown in fig. 8b and 9b.

6. – The internal wave spectra

To determine the origin of the wavy patterns observed, for example, in the temperature field (fig. 4), different runs have been made for both non-stratified and stratified sea
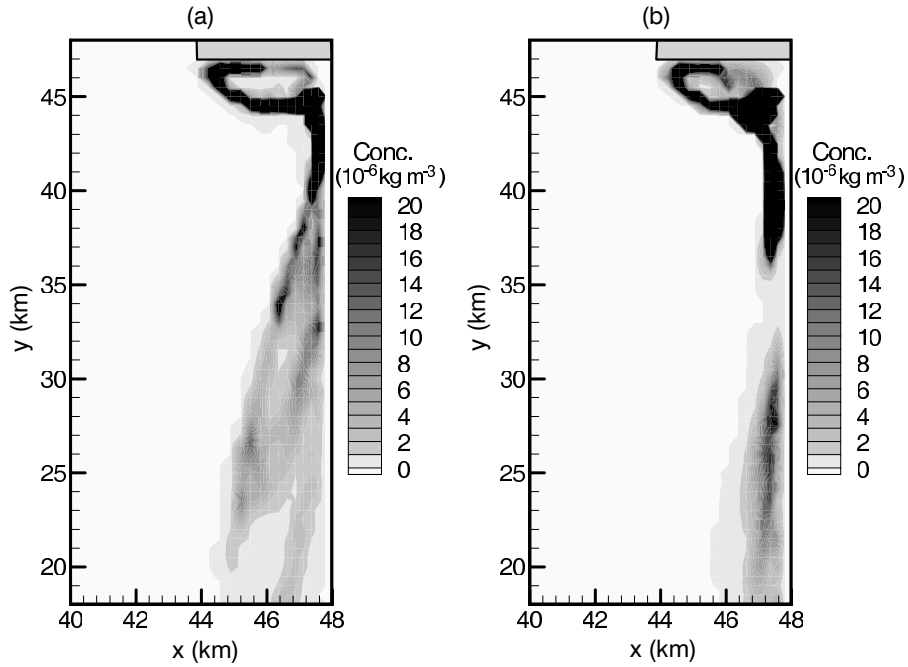
Fig. 8. – Depth-averaged concentrations of pollutant for stratified (a) and isothermal (b) southward current after 6 days of simulation.
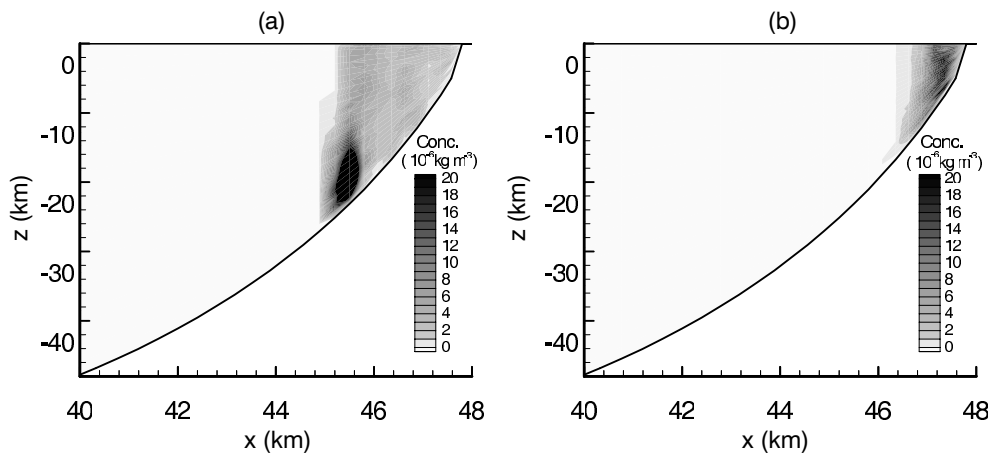

Fig. 9. – Concentrations of pollutant for stratified (a) and isothermal (b) southward current, calculated in a vertical section downstream to the promontory ($y = 27$ km) after 6 days of simulation.
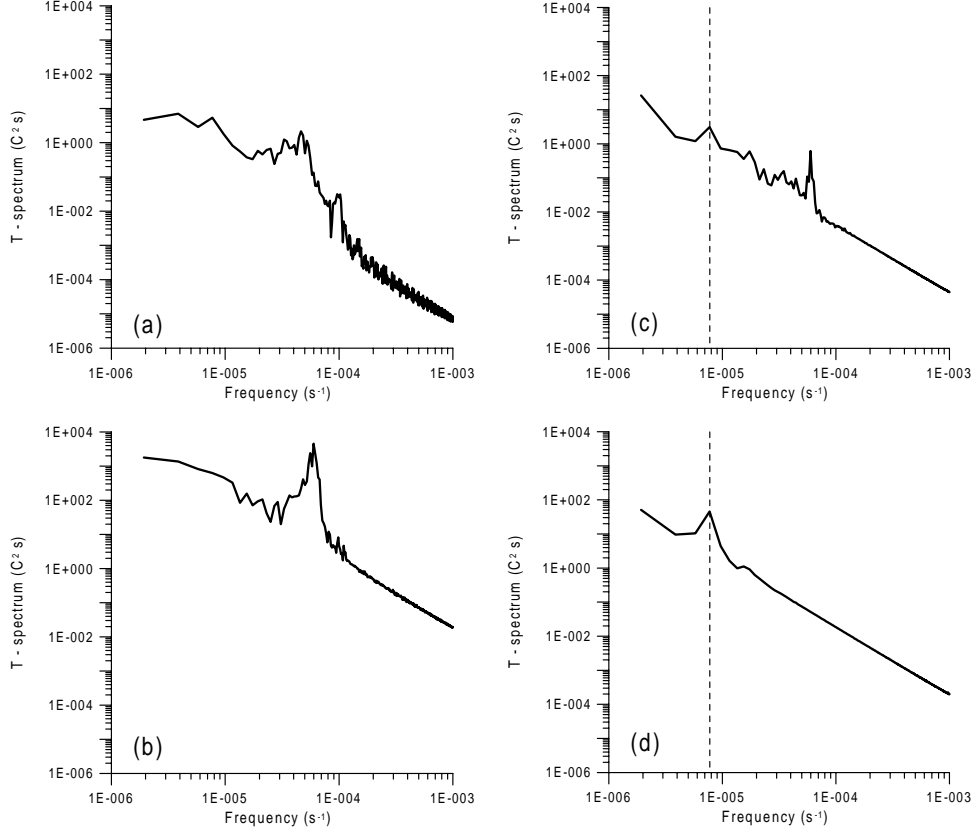
Fig. 10. – Spectra of surface temperature fluctuations for nodes 1 (a), 2 (b), 3 (c) and 4 (d) (fig. 1). Vertical dashed lines mark the vortex shedding frequency f_r.

for: 1) flat; 2) constant slope and 3) present bottom profiles. Since no wavy structure is observed for the non-stratified current for cases 2) and 3), and consequently excluding the topography as forcing mechanisms, it is possible to conclude that the above pattern is determined by IGW, the basic theory of which can be found in classical textbooks [26-28]. We recall that these waves emanate from: 1) the surface; 2) the interior of the ocean and 3) bottom or lateral boundaries [26]. In the present study, only the last mechanisms can be taken into consideration through, for example, the development of the bottom Ekman layer (fig. 5). The following results are referred to the Case A, after 30 days of simulated time, for the 4 surface grid points indicated in fig. 1. The spectra are obtained by dividing the whole time history of temperature fluctuations in 5 segments of equal length, doing the power spectra of each one of the last four segments and averaging them to obtain the averaged power spectrum. The exclusion of the first segment is needed for taking into account the spin-up time of the model.

Figures 10a-d show the surface temperature fluctuation spectra corresponding to the chosen grid points (nodes 1,2,3 and 4 in fig. 1). Firstly, the internal wave spectra (thereinafter IWS) belong to the range $f_C < \omega < N$, as the theory dictates. Secondly, a marked difference denotes the open sea spectrum (fig. 10b) from those near shore, before

(fig. 10a) and after (figs. 10c, d) the promontory ones. In fact, while the node 2 spectrum shows a well-defined peak of the IGW at the frequency 6×10^{-5} s^{-1} (fig. 10b), that lee of the promontory is characterized by the presence of a unique peak corresponding to the value of 7.7×10^{-6} s^{-1} (fig. 10d), *i.e.* the frequency f_r of the vortex shedding defined in sect. **3**. In fact, since the bottom Ekman layer homogenises vertically the temperature field, and then inhibits the development of IGW, the temperature fluctuations can be produced only by the vortex street lee of the headland (fig. 2). It is interesting to note that spectra for node 3 (fig. 10c) seems the result of an overlapping, with a lower total power content, of the previous two kinds because of the presence of both IWS and the vortex shedding peak. No noticeable difference is observable for IWS at the same grids points but for a depth equal to the 40% of the total one.

7. – Conclusions

When the morphological complexity of a marine coastal site is coupled with the presence of a source of pollutants, the environmental impact assessment becomes a hard task the solution of which needs the proper matching between numerical modeling and experimental observations. In this context, the main goal of the present study is to provide a first insight to modeling aspects by coupling a three-dimensional hydrodynamical model (POM) with a three-dimensional Lagrangian stochastic model (LASEMOD) to simulate the dispersion of pollutants released in the southern side of a promontory. In spite of the simplifying conservative assumption, the present study shows clearly how the pollutant dispersion is depending on the inherent structure of the coastal jet, namely its direction and stratification. Moreover, it is shown that the flow generates IGW, whose spectra are closely depending on the grid point position. In particular, those past the promontory show a well-defined frequency that can be described in terms of vortex shedding. Further efforts will be made to collect marine data in the area around the Argentario promontory to validate the present coupled numerical models with observations.

REFERENCES

[1] HAIDVOGEL D. B. and BECKMANN A., in *The Sea*, edited by BRINK K. H. and ROBINSON A. R., Vol. **10** (J. Wiley & Sons) 1998, pp. 457-482.
[2] DOGLIOLI A. M., MAGALDI M. G., PEZZULLI L. and TUCCI S., *Aquaculture*, **231** (2004) 215.
[3] MONTI P. and LEUZZI G., *Boundary-Layer Meteorol.*, **80** (1996) 311.
[4] LEUZZI G. and MONTI P., *Atmos. Environ.*, **32** (1998) 203.
[5] BLUMBERG A. F. and MELLOR G. L., in *Three-dimensional coastal ocean models*, edited by HEAPS N., Vol. **4** (AGU, Washington D.C.) 1987, pp. 1-16.
[6] ORLANSKI I., *J. Comput. Phys.*, **21** (1976) 251.
[7] FLATHER R. A., *Mem. Soc. R. Sci. Liege, Ser. 6*, **10** (1976) 141.
[8] SIGNELL R. P. and ROCKWELL G. W., *J. Geophys. Res.*, **96** (1991) 2561.
[9] BOYER D. L., CHEN R., CHABERT D'HIÈRES G. and DIDELLE H., *Dyn. Atmos. Oceans*, **11** (1987) 59.
[10] BOYER D. L. and TAO L., *J. Fluid Mech.*, **180** (1987) 429.
[11] DAVIES P. A., BESLEY P. and BOYER D. L., *Dyn. Atmos. Oceans*, **14** (1990) 497.
[12] KLINGER B. A., *Dyn. Atmos. Oceans.*, **19** (1993) 27.
[13] PENVEN P., ROY C., COLIN DE VERDIÈRE A. and LARGIER J., *Ocean. Acta*, **23** (2000) 615.
[14] CROMEY C. J., NICKELL T. D. and BLACK K. D., *Aquaculture*, **214** (2002) 211.

[15] HUNTER J. R., CRAIG P.D. and PHILIPS H. E., *J. Comput. Phys.*, **106** (1993) 366.

[16] MEAD C.T., in *3rd International Conference on Marine Waste Water Discharges and Marine Environment, Catania 2004*, edited by AVANZINI C. (MWWD) 2004, proceedings on CD.

[17] THOMSON D. J., *J. Fluid Mech.*, **180** (1987) 529.

[18] STULL R. B., in *An Introduction to Boundary Layer Meteorology* (Kluwer Academic Publishers, Dortrecht) 1994, pp. 360-373.

[19] TAYLOR G. I., *Proc. London Math. Soc.*, **20** (1921) 196.

[20] PICCO P., in *Climatological Atlas of the Western Mediterranean* (ENEA) 1990, pp. 200-210.

[21] TRITTON D. J., in *Physical Fluid Dynamics* (Van Nostrand Reinhold Co.) 1997, pp. 23-25.

[22] PEDLOSKY J., in *Geophysical Fluid Dynamics* (Springer Verlag) 1977, pp. 378-386.

[23] ASTRALDI M. and MANZELLA G., *Cont. Shelf Res.*, **2** (1983) 183.

[24] CUSHMAN ROISIN B., in *Introduction to Geophysical Fluid Dynamics* (Prentice Hall) 1994, pp. 251-259.

[25] MELLOR G. L. and YAMADA T., *J. Atmos. Sci.*, **31** (1974) 1791.

[26] LEBLOND P.H. and MYSAK L. A., in *Waves in the Ocean* (Elsevier Pub.) 1978, pp. 40-53.

[27] GILL A. E., in *Atmosphere-Ocean Dynamics* (Academic Press) 1982, pp. 131-146.

[28] PEDLOSKY J., in *Waves in the Ocean and Atmosphere* (Springer Verlag) 2003, pp. 59-74.